Statistical observations of the trajectories of neutrally buoyant floats in the North Atlantic

by H. J. Freeland,[2] P. B. Rhines[1] and T. Rossby[2]

ABSTRACT

This is a report of the statistical behavior of neutrally buoyant SOFAR floats, drifting at 1500 m depth in the Sargasso Sea where the currents are dominantly time-dependent. The float level is fairly typical of the deep ocean below the main thermocline.

Westward propagation of streamline patterns was unambiguously present over a 180 day period, at an average speed of 5 cm/sec. This exceeded the r.m.s. particle speed (4 cm/sec) and far exceeded the mean westward flow ($\simeq$0.9 cm/sec).

The spatial correlation functions are calculated, and show significant anisotropy of the spatial scales. This anisotropy may be related to the direction of the energy flux in the MODE area.

Maps of the time-averaged intensity and anisotropy of the currents show that, even after eighteen months, there remain strong spatial gradients of kinetic energy density on the 100 km scale, decreasing eastward, especially abruptly at the transition from a flat to a hilly sea-floor, and increasing both northward and southward from the center of the experiment (28°N, 69°40′W).

The polarization of the time averaged currents was significant and quickly varying in space. Such striking 'fine-structure' in the eddy field suggests strong topographic control, both by the irregular shape of the nearby continental rise, and the variations of sea-bed roughness and slope. Even linear planetary waves can show this complex behavior if subjected to irregular ocean bottom and margins.

The Lagrangian auto-covariance function is calculated, and provides a measure of lateral diffusion by the energy-containing eddies, particularly relevant to the Mediterranean salt tongue which intersects this region. Nevertheless the detailed history of the floats is richer than implied by a simple diffusion.

The Lagrangian frequency spectrum has a first moment corresponding to a 51 day period, which may be taken as characteristic of the energy-containing eddies. The Eulerian frequency spectrum, from current meters, has a first moment corresponding to a 54 day period, similar to the Lagrangian value.

Other Eulerian-Lagrangian comparisons suggest agreement in measurements of the average energy density, differences in the shapes of the frequency spectra, and some uncertainty in the time and space averaged currents. Long float-drifts are well-suited to measuring mean currents, except for a bias due to spatially varying eddy intensity, and a possible bias due to their imperfectly Lagrangian nature.

1. Woods Hole Oceanographic Institution, Woods Hole, Massachusetts, 02543, U.S.A.

2. Woods Hole Oceanographic Institution, Woods Hole, Massachusetts, 02543, U.S.A. Present address: Graduate School of Oceanography, University of Rhode Island, Kingston, Rhode Island, 02881, U.S.A.

In all, three independent measures of the non-linearity of the current field are given. The ratio of rms current speed to pattern propagation speed, 0.8, suggests marginally linear dynamics, as does the ratio of the Eulerian to Lagrangian time scales, 1.0. The ease with which mixing of fluid particles occurs, fully comparable to random walks of the same time and velocity scales, indicates a rather stronger level of non-linearity.

1. Introduction

A large number of neutrally buoyant floats were launched in a small region of the N. Atlantic Ocean as part of the Mid-Ocean Dynamics Experiment (MODE). The floats were launched in a region which is roughly square (600 km × 600 km), centred on 28°N and 69°40′W, and at a nominal depth of 1500 m, near the axis of the SOFAR channel. A qualitative description of the floats, tracking system and float trajectories is presented in paper (I) by Rossby, Voorhis and Webb (1975). The purpose of this note is to present the results of a more detailed examination of the float trajectories, including some statistical observations and dynamical inferences.

Most of the floats were launched during the period of the main MODE field program extending from March to mid-July 1973 (MODE-1). However, records from seven trajectories which resulted from initial trials starting in September 1972 and running up to March 1973 (MODE-0), and records from twelve trajectories extending from mid-July to December 31, 1973 (MODE-$1^1/_2$) were used for the purposes of this paper. Hence the data used in most of this report extends from September 1972 to December 1973 and comprises a total of 3614 float-days of observations.

The data base consists of positions of the floats nominally at 4 hour intervals. This has to be qualified since occasional gaps, usually less than a day in length, appear in the data. The gaps were filled by interpolating positions linearly. This process is mainly for convenience in the later handling of the data. Gaps were very rare and it is unlikely that any other process would produce an observable change in any of the following results. After the gaps were filled, velocity time series were produced by differencing the positions, filtering with a low-pass Gaussian filter (half power point at a period of two days) and subsampling at one-day intervals. The resulting velocity time series for each float were used throughout in deriving the following results, except for the Lagrangian spectra in which frequencies up to and including inertial periods were kept.

It should be noted at this point that the motions of the neutrally buoyant floats are not strictly Lagrangian, since a water parcel, in a steady, non-diffusive environment, is constrained to move along σ_t surfaces whereas floats more nearly remain on isobaric surfaces. The 3-day averaged vertical shear at 1500 m does not often exceed 5 cm/sec/1000 m (Leaman and Sanford, 1975). If surfaces of constant potential density move through ± 50 m or so, this implies a maximum error of 0.25 cm/sec, 6% of the r.m.s. speed, probably more than actually occurs. But if this error accumulates it could override the true long-term mean fluid velocity. This is probably

the most serious uncertainty about the instrument, and one that could be more severe in regions of greater vertical shear, greater vertical motion, and in experiments of longer duration. Experiments carried out in the Gulf Stream may suffer such difficulties.

In most of the calculations the data is analysed on an Eulerian basis, i.e. we do not use the fact that the identity of each float is preserved throughout its life. For these the quasi-Lagrangian difficulty is obviated.

2. Prime statistics

From the velocity time series the velocity averages for all floats up to 31 Dec.'73 are $\underset{\sim}{\bar{u}} = (\bar{u}, \bar{v}) = (-0.9, -0.3)$ cm/sec. If we separate the velocity time series into mean and fluctuation components, i.e. $u = \bar{u} + u'$, then we can compute the variances $\overline{u'^2} = 6.8$, $\overline{v'^2} = 8.3$, $\overline{u'v'} = -0.8$ cm^2/sec^2, and we therefore find the r.m.s. speed to be 4.0 cm/sec. Later in this paper the auto-covariance function (acf) of the velocity time series will be discussed; however, it is useful at this point to note that the *acf* has an integral time scale of about 10 days. If we use this as an estimate of the time required for one independent observation of the velocity, then we have approximately $N = 361$ statistically independent observations of the velocity. This, however, assumes that all float tracks are statistically independent of each other. Examination of the tracks of floats 4 and 12 launched in Nov. 1972 (see I) shows considerable visual similarity of nearby float trajectories. If it be assumed that information from one track is redundant when a pair of floats are closer than, say, 55 km, then N is reduced by about 15% to 307. If the variance of a signal is known to be s^2 then the 95% confidence intervals are given by the t-test to be $\pm 2s/\sqrt{N}$. Hence, $\underset{\sim}{\bar{u}} = (-0.9, -0.3) \pm (0.3, 0.3)$ cm/sec. Thus the mean drift of the floats in the MODE region is certainly towards the west, but the north/south component is not different from zero at the 95% confidence level.

There are interesting difficulties, however, in the inference of 'mean-flow' information from ensemble averaged float velocities. A time-averaged flow of large spatial extent will be equal to the instantaneous average over many widely dispersed floats, if the turbulence is homogeneous and stationary. But if the eddy intensity varies in space, as it happened to do in the MODE region, the center-of-mass of the float cluster will move up the gradient of turbulent energy. This false indication of 'mean flow' may have occurred after Dec. 1973 when floats broke away from the cluster and travelled southward at greater than 10 km/day. Rossby et al (I) plot the southward velocity averaged over all floats, and this rose to about 3 cm/sec for about 15 days. A simple model of this bias is the molecular diffusion equation for a concentration C,

$$C_t = \nabla \cdot (K \nabla C).$$

Multiplying by $\underset{\sim}{x}$ and integrating over all space we easily find that, with variable diffusivity, K, the center-of-mass, $\underset{\sim}{\bar{x}}$, of a concentration cloud moves according to

$$\frac{d}{dt}\bar{\underset{\sim}{x}} = \overline{\nabla K} \equiv \int_s C \nabla K \, ds / \int_s C \, ds$$

in the total absence of advecting flow. This discrepancy takes particular significance, for the mean flow indicated by the floats is not consistent with a model of the North Atlantic circulation at 1500 m developed by Worthington (private communication).

The correlation between u' and v' is computed to be negative, but not different from zero at any reasonable confidence level. However, it will be shown that this statistic is strongly space-dependent, and cannot be characterised by a single value.

The ratio, r, of the variance of N/S velocities to the variance of E/W velocities also varies in space. Over this data set it is measured to be $r = 1.2$. Using a one-sided F-test we reject the hypothesis $r > 1$ at the 95% level, but accept it at the 90% level. In a smaller geographical area, r can differ significantly from unity even after considerable time averaging.

3. Spatial correlation functions

The coverage of space by the SOFAR floats is very good at a wide variety of horizontal length scales, and so it was decided to estimate the dominant length scales of the eddies. This can be done most easily by computing the spatial correlation functions. Suppose that at some time, t, two floats are separated by a displacement vector $\underset{\sim}{\xi}$ and have velocities $\underset{\sim}{v}_1$ and $\underset{\sim}{v}_2$ respectively. The components of velocity parallel to (v_{p_1} and v_{p_2}) and transverse to (v_{t_1} and v_{t_2}) the displacement vector $\underset{\sim}{\xi}$ are computed, and the contributions $v_{t_1} v_{t_2}$ and $v_{p_1} v_{p_2}$ to the transverse and longitudinal covariance functions are accumulated for the specific displacement vector $\underset{\sim}{\xi}$. The calculated covariances are then averaged over all time and over 25 km squares in displacement space (the spatial resolution). The mean velocity computed from the ensemble of floats was subtracted from each velocity time series. The available data are sufficient for this type of calculation, but inevitably a few (fortunately *very* few) points in displacement space yielded covariances with very small weights. (Weight was defined here as the total number of float-pair days). Thus, a smoothing operation was applied which replaced the covariance $C_{i,j}$ at position $(x,y) = (i\Delta, j\Delta)$, (where $\Delta = 25$ km or the resolution of displacement) by a weighted mean $\bar{C}_{i,j}$ of the nearest neighbours in the covariance array. Specifically

$$\bar{C}_{i,j} = \frac{4 W_{i,j} C_{i,j} + W_{i+1,j} C_{i+1,j} + W_{i-1,j} C_{i-1,j} + \cdots\cdots}{4 W_{i,j} + W_{i+1,j} + W_{i-1,j} + \cdots\cdot}$$

($W_{i,j}$ is the weight associated with the covariance at position $(i\Delta, i\Delta)$). The resulting covariances were then normalized by the directionally dependent variance yielding the transverse and longitudinal correlation functions shown in Figs. 1a,b respectively. Because the spatial resolution is 25 km in displacement space, there is no information on the structure of the functions inside the 25 km circle.

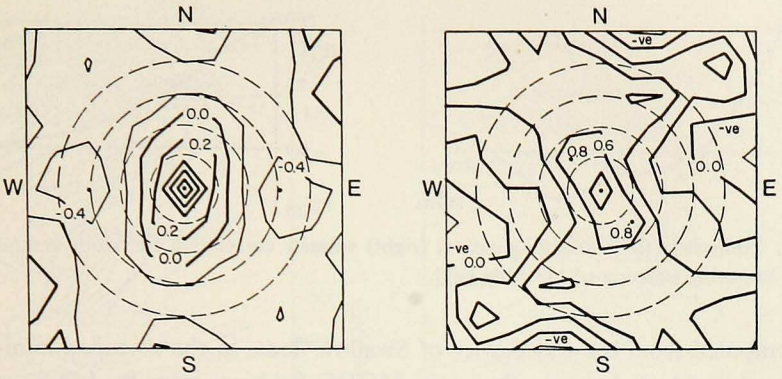

Figure 1. Transverse (1a) and longitudinal velocity correlation functions. Bold lines are contours of positive correlation (or zero) and narrow lines negative. Contouring interval is 0.2; and displacements of 25, 50, 75 and 100 km are indicated by dahsed circles.

The length scales, as determined by the distance to the first zero crossing (r_c) of the transverse function, are considerably shorter than were expected before the MODE field program. The average r_c in Fig. 1a is about 55 km. Compare this with the smallest distance between moorings in MODE, 50 km, which was based on a design assuming an r_c between 75 and 90 km. Both correlation functions indicate considerable anisotropy; the transverse field shows the direction of maximum correlation to be about 0°T and the longitudinal field −30°T. The ratio of maximum r_c (65 km) to minimum r_c (35 km) is about 2. These observations appear to be stable statistics. Correlation functions derived using only 1/3 of the data used here produce remarkably similar results. Specifically the values of r_c agree to about 10% in all directions.

It is well known that for a two-dimensional isotropic field the covariance tensor has a particularly simple form (e.g. Lumley & Panofsky, 1964) viz.

$$R_{ij}(\xi) = \overline{u_i(\underset{\sim}{x})u_j(\underset{\sim}{x}+\underset{\sim}{\xi})} = \sigma^2\left[\frac{f(\xi)-g(\xi)}{\xi^2}\xi_i\xi_j + g(\xi)\,\delta_{ij}\right].$$

[Where $f(\xi)$ and $g(\xi)$ are the one-dimensional longitudinal and transverse correlation functions and ξ is written for $|\underset{\sim}{\xi}|$]. If the field be non-divergent then $R_{ij,i} = 0$, and for two-dimensional flow we find that

$$g(\xi) = \frac{d}{d\xi}[\xi f(\xi)]. \tag{3.1}$$

Fig. 2 shows the results of an attempt to test the hypothesis of non-divergence in two dimensions by using the above relation. The points shown are values of the transverse and longitudinal correlation functions $g(\xi)$ and $f(\xi)$ derived by averging the anisotropic functions in circles around the origin. The values at small separations

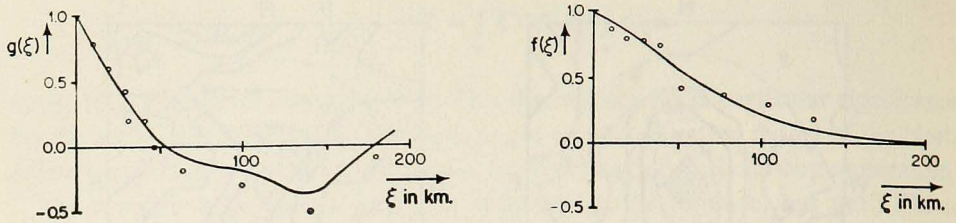

Figure 2. Transverse (left) and longitudinal (right) velocity correlation functions computed from Fig. 1 imposing isotropy of the eddy field.

were computed from the trajectories of Swallow floats in the so-called mini-MODE experiment conducted within the main MODE field program by I.O.S. scientists. [These results were kindly made available by Dr. J. Swallow]. A smooth curve was constructed which fitted the points representing $g(\xi)$ and this was digitised. Correlation functions must be positive definite, but the digitised version of $g(\xi)$ did not fulfill this criterion. So, $g(\xi)$ was forced to be positive definite by computing the Fourier transform of $g(\xi)$, setting the negative energies equal to zero and transforming back again. The resulting model of $g(\xi)$ was then integrated to compute $f(\xi)$. The solid lines in Fig. 2 are two positive definite correlation functions related and computed as above. It does appear from this comparison that the flow field is substantially non-divergent, as was expected. It remains to be seen, however, what is the effect of the observed anisotropy on this statistical test of 2-D non-divergence.

4. Phase propagation

The stream function field was computed, at three-day intervals, from the float velocity data using the technique of objective analysis. These maps of the stream function field will be published shortly in a separate paper (Freeland and Gould, 1976). Casual inspection of the maps shows a general westward drift of the pattern of eddies which can most clearly be seen on a time-longitude plot. For each map the positions of streamlines were marked on the 28°N latitude, and the stream function was then contoured in the longitude-time plane, shown in Fig. 3a. Similarly the stream function field was contoured in the latitude-time plane, for longitude 69°40′W, shown in Fig. 3b. Referring now to Fig. 3a we see a well-defined slant to the streamlines. The bold lines, indicating the paths of zeros of N/S velocity on the 28°N latitude, also indicate a westward drift of the eddy pattern at a speed ranging from 2 to 10 cm/sec. A trend analysis (Longuet-Higgins, 1957) which weights energetic periods more heavily than others, yields a mean westward phase speed of 5 cm/sec at 69°40′W, the center line of the phase plot. The N/S section shown in Fig. 3b has a completely different character. There is no evidence of any systematic motion to the eddy pattern in the N/S direction.

This observation has several important ramifications. Westward propagation is the most nearly ubiquitous property of the beta-plane. Numerical models (e.g.,

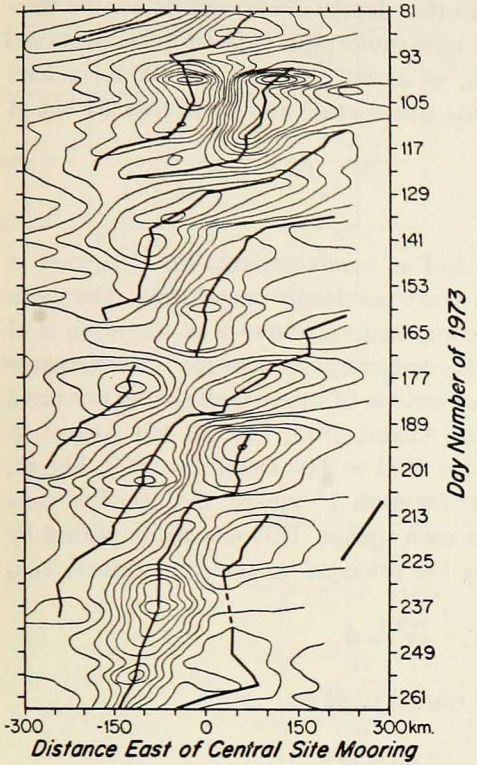

Fig. 3a.

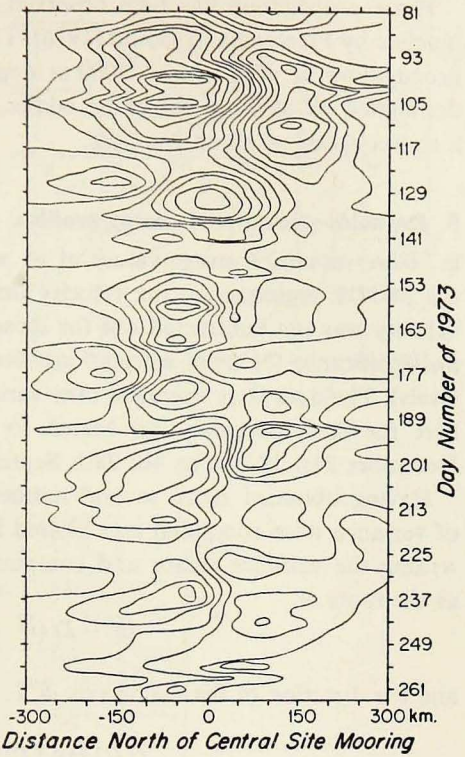

Fig. 3b.

Figure 3. Contours of streamfunction in the plane of time (downwards) and distance along a section through the MODE region (horizontal axis). Fig. 3a is a time-longitude plot and 3b a time-latitude plot. A slope of 5 cm/sec is indicated by a bold line on 3a.

Rhines, 1975) show such phase tendency even well into the nonlinear range where significant wavenumber cascades of energy may be occurring. The ratio of rms particle speed to the phase speed, of order unity, is an estimate of the wave-steepness of the eddy-like motions, or the degree of non-linearity. In deep water, below the thermocline, in order that a well defined phase propagation be observable, we require that lines of constant f/H resemble lines of constant f, i.e. a dynamically smooth bottom. This suggests that the environment centered on the Hatteras abyssal plain, which is only 200 km wide, is dynamically smooth. There is no evidence in the phase plots of a difference between the rough and smooth regions, because the data are rather sparse over the rough topography. The r.m.s. particle speed is about 4.0 cm/sec, somewhat less than the phase speed, and the mean westward flow, 0.9 cm/sec, is considerably less than either. This immediately suggests that phase motion was observed which is not simple advection westwards but involves some genuine propagation of phase by a wave-field.

Phase propagation has been observed at other depths above and below the thermocline by Freeland and Gould (1976). Time-longitude plots indicate a fast westward propagation at 4000 m and 3000 m depth, of about 5 cm/sec. At 500 m, a level dominated by shallow baroclinic eddies, the phase again moves westwards but at a slower speed of about 2 cm/sec.

5. Reynolds stresses and energy profiles

a. Observations. Average values of u^2, v^2, and uv were computed for 1° squares in the MODE region using the velocity time series previously constructed. The mean velocity was not subtracted out for these computations (removal of the mean is of no significance for most calculations, but becomes important at low kinetic energy levels). The data were averaged over various periods of time, results being presented here for three periods: 12th March to 6th August 1973, Fig. 4a; 6th August to December 31st 1973, Fig. 4b; 28th September 1972 to 31st December 1973, Fig. 4c.

Having obtained mean second moments for each 1° square, the principal axes of variance were computed and plotted for each square. This was accomplished by writing the variance tensor and computing the principal values (eigenvalues) λ_1,λ_2 as the roots of

$$(\overline{u^2} - \lambda)\,(\overline{v^2} - \lambda) - \overline{uv}^2 = 0,$$

and the direction of the major axis, θ°T, is related to $\overline{uv}$ by

$$(1/2)\tan(2\theta) = \overline{uv}/(\overline{v^2} - \overline{u^2}).$$

The number in the upper left of each 1° box is the statistical weight in float-days. Once again we estimate the equivalent number of degrees of freedom as weight/10. This is probably rather conservative, a more pragmatic way of checking the statistical stability of observations is to compare the axes of Fig. 4a with those of 4b, computed from independent sets of data. Wherever the weight is reasonably large the resemblance between the two diagrams is good. The axes on the far right of each figure are computed from the averages for each row; the bottom set for column averages. Comparing the row averages of Figures 4a and 4b it is striking that the principal directions are reproduced almost perfectly, though the kinetic energy (proportional to the sum of the major and minor axes) shows a consistent increase in the later time period.

On Figure 4c five additional sets of axes have been added, for comparison, derived from the MODE current meter records. The weights associated with these axes are comparatively low, averaging about 50 data days each. (The numbers beside each set of current meter axes identifies the W.H.O.I. or I.O.S. record number).

Three isobaths have been added to Figure 4a,b,c for reference, at depths of 5000 m, 5400 m, and 5400 m (reading from left to right), and are chosen to indicate the principal bathymetric regimes of the MODE area. Between the 5000 m and 5400 m

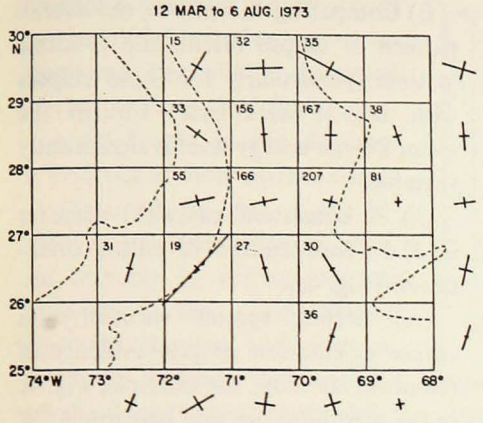

Fig. 4a.

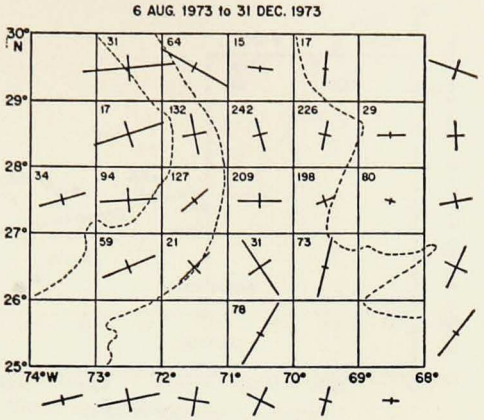

Fig. 4b.

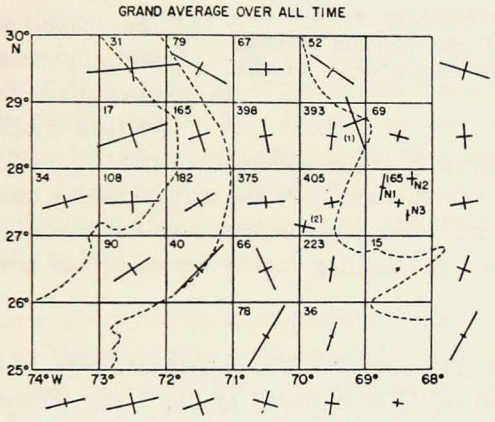

Fig. 4c.

Figure 4. Principal axes of the variance tensor plotted against position in the MODE region for two independent time periods a,b and for the period September 1972 to December 1973, c. Axes labelled 1 and 2 are WHOI current meter records 5015 and 4955 respectively and N1, N2, and N3 are IOS current meter records, all at 1500 m depth.

isobaths we have the outer slopes of the Blake-Bahama Rise, the steepest slopes in the MODE region. The central region between the two 5400 m isobaths is the abyssal plain which is extremely flat and smooth. To the east we have a rougher topography, small hills that rise out of the sediment cover of the abyssal plain. There is a mean slope of about 3.0 metres/km (depth decreasing to the east) associated with the rough topography.

b. Discussion. There are several interesting features in Fig. 4 which deserve description.

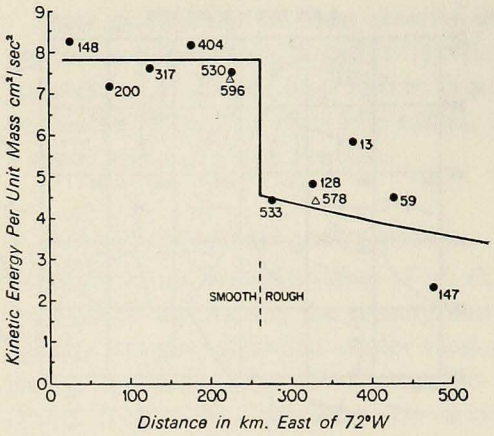

Figure 5. Variation of kinetic energy density versus distance east of 72°W. Data derived from float trajectories indicated by •, and data derived from WHOI site moorings indicated by △. The numbers indicate 'weight' of each point in data-days.

(i) Comparing 4a with 4b, the overall pattern of ellipse orientation is stable in time (particularly for those ellipses with largest data base) though the mean kinetic energy level is significantly variable.

(ii) A consistent eastward decrease in *K.E.*, independent of ellipse orientation (Fig. 4c).

(iii) Strong spatial variability in ellipse orientation despite evidence of temporal stability; for example, Fig. 4c in the meridional section between 70°W and 71°W.

(iv) The ellipses near the outer slope of the Blake-Bahama outer rise are significantly polarized parallel to the trend of the isobaths.

We then conclude that there is evidence that the bathymetry is controlling the orientation of at least some of the axes. However, the overall stability of the ellipse pattern needs to be explained; it is not that eddies are 'locked' in position over the abyssal plain by topographic features, for they are propagating rapidly (phase speeds around 5 cm/sec) across the abyssal plain.

c. Kinetic energy profiles, east-west. The spatial variability of kinetic energy plotted against distance east of 72°W is shown in Fig. 5. The circles indicate the kinetic energy per unit mass averaged over all floats passing through meridional bands 50 km wide and centred on the circle. The triangles are the equivalent observations derived from MODE site mooring records at a depth of 1500 m. (The information for these points was kindly made available by Dr. W. Schmitz). Note once again that one degree of freedom is about 10 days, so there is little reliability associated with the point having a weight of only 13 float-days. There is little doubt that there is a strong gradient in the kinetic energy density, with energy decreasing to the east. However, casual inspection of the profile shows that the variation is not simple. The transition between the rough and the smooth topographic regimes is indicated on Fig. 5, and we see that over the rough area there does appear to be some decay in *K.E.*; over the smooth area there is no evidence of a decay; at the boundary between the two regimes there appears to be a discontinuity in kinetic energy. The solid line drawn in on Fig. 5 is only meant to be a sketch of the possible kinetic energy variation; however, it does appear that the kinetic energy level is somehow topographically determined. It is not difficult to think of a model of wave-topo-

graphy interaction which would produce this kind of energy variation, and this will be discussed further at the end of this paper.

North-South. In Fig. 4c there is evidence of more intense eddies at the northern edge of the region, in agreement with the general increase in activity as one approaches the Gulf Stream (Schmitz, Luyten and Sturges, 1975). In addition the behavior of the floats later in their drifts suggest that there may be a steep rise in energy *southward* of the MODE center. In the first three months of 1974 several floats escaped the main cluster and raced southward (see I). When time- and longitude-averaged *K.E.* is plotted against latitude, Fig. 6, these events produce a large gradient up to a maximum of about four times the average (MODE area) energy, near the Antilles barrier. This surge of energy did not occur at anything like this level at the MODE center (where there were two site moorings with current meters) and so the event was not purely temporal. To be sure the data base far to the south of the MODE center is small, but there is a possibility that this area is permanently energetic.

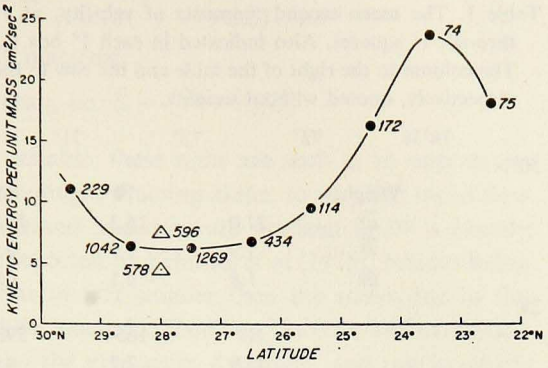

Figure 6. Variation of kinetic energy density versus latitude. (See Fig. 5 caption).

d. Dynamics. We have established that large gradients in the intensity and polarization of currents exist in the 'mid-ocean', and endure for many eddy periods. These form a fine-structure (at a scale $\simeq$ 100 km) coexisting with the basin-wide variation in properties which Schmitz et al (1975) are mapping. A permanent, small-scale structure was not anticipated, it seems unfamiliar, and it presents severe problems to those who wish to make global maps of second-order statistics of the currents. Possibly the Lagrangian floats, which roam freely, and sample many different regions, will escape the bias that a moored current meter would find in such a field and thereby escape the fine-structure 'difficulty'.

Besides this intrinsic interest, eddies can drive timeaveraged currents. For one estimate of this we calculated the gradients of the Reynolds stresses by making a linear (weighted) regression of the data in Table 1, to estimate the spatial derivatives. (The data in Table 1 was used in constructing the principal axes of Fig. 4c).

$$\frac{\partial \overline{u^2}}{\partial x} = -3.0 \times 10^{-7} \qquad \frac{\partial \overline{u^2}}{\partial y} = 0.73 \times 10^{-7}$$

$$\frac{\partial \overline{v^2}}{\partial x} = -0.73 \times 10^{-7} \qquad \frac{\partial \overline{v^2}}{\partial y} = 0.02 \times 10^{-7}$$

Table 1. The mean second moments of velocity, $\overline{u^2}$, $\overline{v^2}$ and $\overline{uv}$ averaged over all floats passing through 1° squares. Also indicated in each 1° box is the number of float-days of observations. The column to the right of the table and the row to the bottom are the row and column averages, respectively, quoted without weights.

	74°W	73°	72°	71°	70°	69°	68°	
30°N								
		Weight	31	79	67	52		
		$\overline{u^2}$	27.0	15.3	10.6	12.7		15.1
		$\overline{v^2}$	7.9	7.9	4.5	9.3		7.1
		$\overline{uv}$	1.8	− 6.1	0.0	− 4.6		− 2.8
29°								
			17	165	398	393	69	
			20.9	7.7	4.0	3.7	5.6	4.9
			9.1	10.4	10.3	8.7	4.0	8.0
			4.3	− 1.1	− 1.2	0.6	− 0.4	− 0.4
28°								
		34	108	182	375	405	165	
		13.8	16.5	8.4	11.2	5.0	3.0	8.3
		4.5	7.1	5.2	4.1	4.2	2.5	4.3
		2.9	0.4	3.2	0.6	0.2	− 0.1	0.8
27°								
			90	40	66	223	15	
			10.4	12.2	5.8	2.1	0.6	5.1
			7.3	12.6	11.9	8.0	1.3	8.4
			3.6	8.6	− 3.7	0.9	0.4	1.4
26°								
					78	36		
					7.5	1.7		5.3
					16.6	8.5		13.3
					8.7	2.7		6.4
25°								
		12.0	15.5	9.6	7.6	4.2	3.5	
		3.4	7.2	8.1	8.2	6.9	2.8	
		2.2	2.0	0.6	0.2	0.3	− 0.1	

$$\frac{\partial \overline{uv}}{\partial x} = -0.46 \times 10^{-7} \qquad \frac{\partial \overline{uv}}{\partial y} = -1.5 \times 10^{-7}$$

(all in cm/sec²).

If typical of the entire water column, the first of these (the largest) would represent a stress of 0.17 dyne/cm². Note that the steep east-west gradient, Fig. 5, was smoothed by this process; if it had not been, a local value of $\partial \overline{u^2}/\partial x$ several times as large would have resulted.

Using $\bar{\underset{\sim}{u}} = (-0.9, -0.3)$ cm/sec we find

$$\frac{\partial \bar{E}}{\partial t} = -\bar{u}\frac{\partial \overline{u^2}}{\partial x} - \bar{u}\frac{\partial \overline{uv}}{\partial y} - \bar{v}\frac{\partial \overline{uv}}{\partial x} - \bar{v}\frac{\partial \overline{v^2}}{\partial y} + \text{other terms}$$

$$= (-2.7 \quad -1.3 \quad -0.13 \quad +0.0) \times 10^{-7}$$
$$= -4.1 \times 10^{-7} \text{ erg/unit mass/sec.}$$

(Here $\bar{E}$ is the kinetic energy of the mean, i.e. $\bar{E} = (\overline{u}^2 + \overline{v}^2)/2$).

Although numerical values are not reliable, these signs are such as to oppose the observed mean flow, and at a rate fast enough, if acting alone, to stop the mean flow in about 13 days. The sign of the observed fine-structure gradient in $\overline{uv}$ is exactly the opposite of the gyre-scale gradient reported by Schmitz et al (1975), besides being very much larger in magnitude. (It was in fact smaller than the stress due to the east-west gradient in intensity). It must be concluded then that the observed variations pose a problem in the local, rather than the gyre-scale, dynamics, and one in which the 'other terms' in the above equation are active. The sign of the observed N/S gradient in $\overline{uv}$ cannot be maintained over a distance very much larger than the MODE region without introducing serious discrepancies with other observations. Further remarks on eddy-mean flow interactions are given in 6.

6. Temporal aspects

a. Lagrangian diffusion. The experiment provided a generous number of nearly Lagrangian trajectories, and this aspect is of value far beyond the use of SOFAR floats as drifting current meters. The results are relevant to both tracer distributions and to dynamics.

The problem of the diffusion of a cloud of marked particles depends heavily on the Lagrangian autocovariance, defined here as:

$$R_{ij}(\tau, T, t_0, \underset{\sim}{x}_0) = \frac{1}{T}\int_{t_0}^{t_0+T} u_i'(\underset{\sim}{x}_0, t)\, u_j'(x_0, t+\tau)\, dt. \tag{6.1}$$

(Here i and j can take the values 1 and 2 for observations in the x and y directions respectively).

For ideal, homogeneous, stationary fields the limit $T \to \infty$ is taken and dependence on T and $\underset{\sim}{x}_0$ and the initial time, t_0, vanishes to leave the usual covariance function $R_{ij}(\tau)$ of Taylor (1921). Here, despite our demonstration of both inhomogeneity and anisotropy, we proceed as if the simple theory applied; its limitations will become clear.

The mean velocity of the ensemble of all floats was subtracted from the eight longest time series, of floats that remained in the central MODE area, and the residual fluctuation series were used to compute the covariance tensor for each 'drift'. The tensors for the eight drifts which ranged in length from 201 to 328 days, were averaged together to yield Fig. 7. The symmetry properties $R_{ii}(\tau) = R_{ii}(-\tau)$, $R_{12}(\tau) = R_{21}(-\tau)$ have been used to omit redundant halves of the curves.

The covariances R_{22} and R_{11} are unequal, consistent with the anisotropy of Fig. 4. They have small, or insignificant negative lobes beyond the first zero crossings,

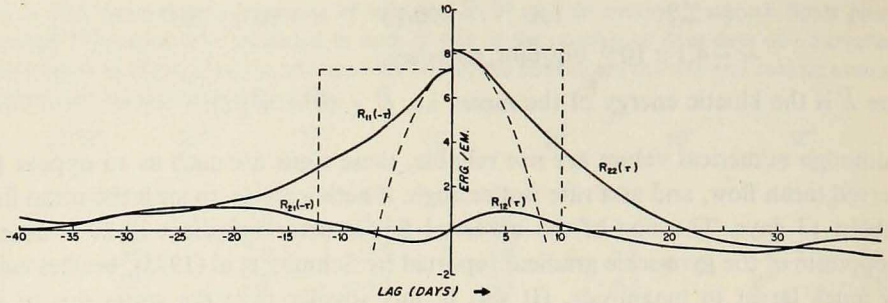

Figure 7. Lagrangian auto-covariance tensor averaged over eight realisations.

which occur at 22 and 40 days respectively. In view of our remarks about wave dynamics, this lack of deep negative lobes is puzzling, for a highly oscillatory field might be expected to develop strong negative correlations.

The covariances $R_{11}(\tau)$ and $R_{22}(\tau)$ are parabolic near the origin. This is expected on theoretical grounds, and implies only that the accelerations are finite. The osculating parabolae are drawn in; the time lags at which these intersect the time axis, 6.8 and 8.4 days for R_{11} and R_{22} respectively, are analogous to the Taylor microscales, λ_1 and λ_2. If the correlations are stationary, then we immediately deduce

$$\overline{\left[\frac{du_i'(t)}{dt}\right]^2} = \frac{d^2}{dt^2} R_{ii}(t)\bigg|_{t=0} = \frac{2R_{ii}(0)}{\lambda_i^2}.$$

[The summation convention for repeated indices is not used in this section.]

Hence, we compute the r.m.s. 'geostrophic' accelerations of u, v, and speed to be 6.3×10^{-6}, 5.6×10^{-6} and 8.4×10^{-6} cm/sec^2 respectively from the microscale measurements. From the original time series, filtered to remove inertial and higher frequencies, the r.m.s. acceleration of speeds is calculated to be 7.3×10^{-6} cm/sec^2, which is in good agreement with the correlation functions.

For a homogeneous field the second moment of the particle displacement varies according to

$$\overline{x_i^2}(t) = 2\int_0^t \int_0^{t'} R_{ii}(\tau)\, d\tau\, dt' \tag{6.2}$$

where the average is or over an ensemble of realizations. Thus, initially the variances $\overline{x_1^2}$ and $\overline{x_2^2}$ grow like t^2, but after an eddy time-scale (20 days or so) has passed, the turbulent diffusion slows to a random walk,

$$\frac{1}{2}(\overline{x_1^2}, \overline{x_2^2}) = t\int_0^\infty (R_{11}, R_{22})\, d\tau.$$

The diffusivities K_{11} and K_{22}, for dispersion in the x and y directions respectively, become, after 20 days

$$K_{11} = \int_0^\infty R_{11}(\tau)\, d\tau$$

and

$$K_{22} = \int_0^\infty R_{22}(\tau)\, d\tau,$$

or simply the product of velocity variance and integral time scale. The computed integral scales of R_{11} and R_{22} are 12.3 and 10.1 days, respectively, indicated on Fig. 7 by the dashed lines enclosing areas equal to the integrals of $R_{ii}(\tau)$. These imply values of the diffusivity of $(K_{11}, K_{22}) = (7.8, 7.1) \times 10^6$ cm^2/sec, which are rather small compared with classical estimates of 1×10^8 to 4×10^8 (Sverdrup, Johnson and Fleming, 1942) for the large scale ocean.

But how accurately do these classical formulas sum up the actual dispersal of the floats. First, as we pointed out earlier, the center of mass of the float cluster does not move with the Eulerian or flow in the region, but is attracted toward regions of intense eddies. A simple model suggests (Rhines, in preparation) that in a field with a slowly-varying correlation function $R_{ij}(\tau; x_1, x_2)$ the center of mass $\bar{x}_i$ moves at a rate $\frac{\partial}{\partial t}\bar{x}_i = \frac{\partial}{\partial x_j}\bar{K}_{ij}$, where $K_{ij} = \int_0^\infty R_{ij}\tau; x_1, x_2)\, d\tau$, and the bar indicates a weighting by the float distribution. This may in part explain the pulse of strong southward flow in early 1974, when the average over all floats reached 4 cm/sec to the south.

Second, the quasi-homogeneous formulas suggest a diffusion which is isotropic, and would extend the cloud of floats laid at the end of the intense MODE-1 experiment, in June 1973, from about 75 km standard deviation to about 215 km standard deviation in 10 months. In fact this describes the average spread fairly well, but there is rather a lot of 'geography' and anisotropy visible in the tracks, as discussed in I; the floats spread first to the west and then to the south of the original center. They were totally unwilling to go north of 30°N (less than a predicted standard deviation from the origin), and reluctant to go east into the abyssal hills. Hence, the trajectories support the conclusions drawn from the Eulerian statistics that some aspect of the inhomogeneity of the ocean, perhaps involving both the large scale topography and the disposition of energy sources, is acting to a significant degree.

It is of some interest to determine whether or not the theory of diffusion by homogeneous turbulence is accurate in even an average sense. Equation (6.2), Taylor's Theorem, represents the starting point for almost all of classical diffusion theory. This relation is a mathematical identity, requiring only homogeneity and stationarity of the statistics; it is, however, instructive to compute the left and right-hand sides of this relation independently and to compare them. The autocovariance function has already been described, and it is a simple matter to carry out the integrations to produce the right-hand side. To compute the left-hand side we look directly at the x and y coordinates of the 43 individual float trajectories. These trajectories had

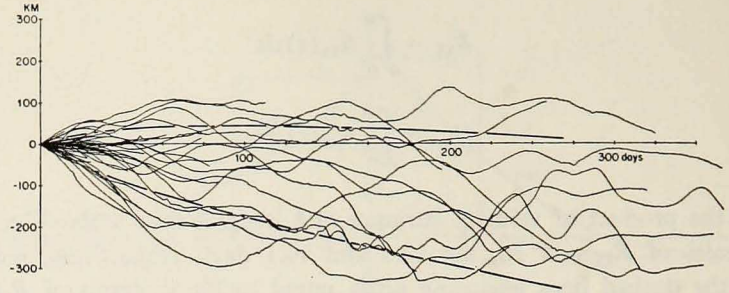

Fig. 8a.

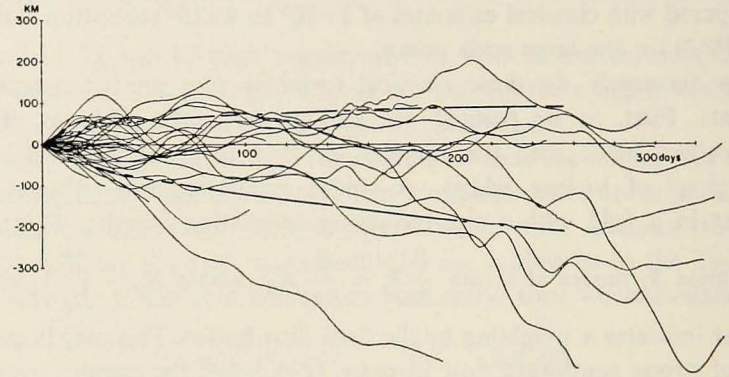

Fig. 8b.

Figure 8. Displacement of floats in E/W and N/S directions, a and b respectively, against time after launch of each float. Bold lines show the expected dispersion (standard deviation about the centre-of-mass) computed by integrating the auto-covariance functions and adding in the mean flow.

their origins at different points in space and time. However, under the simplifying assumptions of statistical homogeneity and stationarity we can substitute spatial averaging for time averaging and regard the float tracks as being equivalent to a large number of tracks originating from one point in space and differing only in the time of launch. Hence, we plot the east/west and north/south displacement of all floats, relative to their launch points, against time after launch, as shown in Figs. 8a,b respectively.

The centre of mass of the float cloud drifts to the south (0.3 cm/sec) and to the west (0.9 cm/sec); this is as should be expected. However, rather than having a parabolic envelope, at large time, the east/west dispersion actually ceases after about 100 days. This is a characteristic of a wave field; to produce this kind of behaviour from the auto-covariance function we require deep negative lobes after the first zero-crossing to reduce the 1st integral of $R_{11}(\tau)$ to zero. Once again, the absence of such lobes in Fig. 7 is surprising. The lack of significant excursions to the north and east is striking, as is the difference in character between the north/south and east/west dispersion. Evidently, the dispersion is not isotropic.

For small times after launch the square of the dispersion (dispersion is the standard deviation of float tracks from the center of mass) varies as

$$(\overline{x^2}, \overline{y^2}) \approx (\overline{u^2}, \overline{v^2})\,\tau^2,$$

according to Eq. (6.2). For small times after launch the floats are all close to their launch points and hence the velocity variances, above, are typical of a relatively small central MODE region. In Fig. 9 we have the dispersion plotted against time for the first 8 days. As expected the dispersion increases linearly with time. However, the slopes of the lines are less than expected, the observed dispersion implies velocity variances of $(\overline{u^2}, \overline{v^2}) = (3.2, 6.6)$ cm^2/sec^2. These are not even close to the values computed directly in the auto-covariance functions, viz. $(\overline{u^2}, \overline{v^2}) = (7.3, 8.2)$ cm^2/sec^2. It might be argued that since most of the floats were launched during a period of a few months in the summer of 1973, we are looking at the dispersion in a rather narrow time period. In contrast the velocity autocovariance functions are computed as averages over entire float tracks, and so are not limited in their coverage of time. In other words, the discrepancy results from the non-stationarity of the statistics. This can be tested. After a suitable time, say 30 days, float velocities are statistically independent of the velocities at launch, and we can regard each 30 day segment of float track as one independent realisation of all possible float tracks in the eddy field. We can, therefore, restart the dispersion experiment every 30 days and get several independent estimates of the velocity variances. These estimates yield $(\overline{u^2}, \overline{v^2}) = (3.9, 6.7)$ cm^2/sec^2, averaged over all estimates, with standard deviations to these estimates of (0.6, 1.5) cm^2/sec^2. Evidently non-stationarity may explain the discrepancy in $\overline{v^2}$ but certainly not in $\overline{u^2}$.

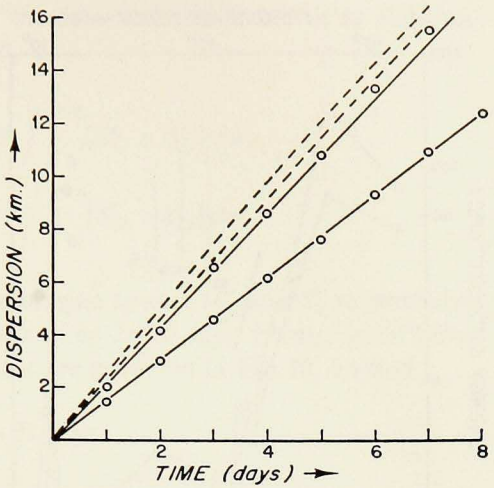

Figure 9. The E/W and N/S measured dispersion (bold lines and circles) and dispersion predicted from the autocovariance functions of Fig. 7. For each pair the lower curve is the E/W dispersion and the upper the N/S dispersion.

It appears that Taylor's Theorem, and by implication classical diffusion theory for nearly homogeneous turbulence, is not capable of describing the dispersion of SOFAR floats in the MODE region. The applicability of classical diffusion theory to oceanic tracer studies is, therefore, moot.

b. Spectra and Eulerian-Lagrangian comparisons. Several very long time series of SOFAR float positions are available resulting from the replacement of fading floats by new floats. These long time series were used for computing estimates of the

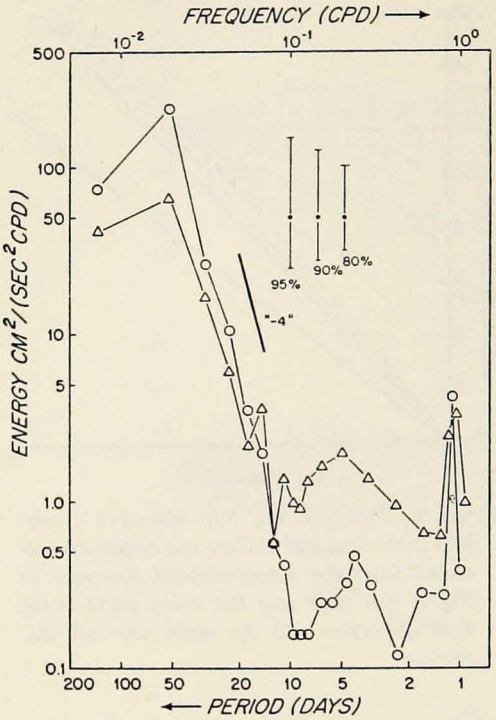

Figure 10. Lagrangian power spectra of N/S and E/W velocities, indicated by ○ and △ respectively. Average number of degrees of freedom each = 10.

Lagrangian velocity spectra. A typical example is shown in Fig. 10 in the range of periods 1 to 150 days. This particular example is taken from the trajectory labelled Link Study 52 in paper (I). The power spectra of u and v time series are plotted independently, the estimates contain 10 degrees of freedom each and the 95%, 90% and 80% confidence intervals are shown for comparison.

For periods greater than about 30 days we have the energy-containing eddy range; between 1 and 10 days there is a deep spectral gap, at a period of about 1 day a strong inertial peak is found. At long periods the energy density in the N/S motion exceeds that in the E/W motion. This is consistently observed in all the float spectra examined. The curves cross and the N/S motion is less energetic in the spectral gap. Apparently this region, 2 to 7 day periods, is dominated by noise in the navigation technique. (The SOFAR float listening stations tend to be arranged north and south of the MODE area so that there is a greater noise level in longitude observations than in the latitude determinations). The slope in the range of periods 30 to 10 days is very large; if $S(\omega) = S_{11}(\omega) + S_{22}(\omega) \propto \omega^{-n}$ then n is somewhat greater than 4. This is also consistently observed. This slope is substantially greater than the slope '-3' usually observed in Eulerian records, e.g. Thompson (1971a), and we expect the spectral gap to be deeper in the Lagrangian data. Small-scale (10 km scale) features can be advected by the energy containing eddies (the spectral peak) leading to a Doppler shift *into* the high frequency region of the Eulerian spectrum, but no such Doppler shift would be expected in the Lagrangian version. In this sense the floats may provide a 'purer' picture of the energy-containing eddies.

Another version of the Lagrangian spectrum is the Fourier transform of R_{11} and R_{22}, Fig. 7. Rather more data (eight tracks) were used to produce Fig. 7, but the spectrum, not reproduced here, is very similar to Fig. 10, except that it continues to rise toward lower frequencies. This is related to the lack of deep negative lobes in the covariance function.

To compare the dominant frequency of the data with that found in an Eulerian (current meter) record, we define $\bar{\omega}_e$ and $\bar{\omega}_l$

$$\bar{\omega}_e = \int_0^{\omega_1} \omega \{S_{11}^e + S_{22}^e\} d\omega \Big/ \int_0^{\omega_1} \{S_{11}^e + S_{22}^e\} d\omega,$$

$$\bar{\omega}_l = \int_0^{\omega_1} \omega \{S_{11}^l + S_{22}^l\} d\omega \Big/ \int_0^{\omega_1} \{S_{11}^l + S_{22}^l\} d\omega$$

as the first moments of the Eulerian and Lagrangian spectra (S_{ii}^e and S_{ii}^l respectively) where ω_1 is the cut-off frequency, here taken to be $2\pi/10$ days. From a set of three compound trajectories, one of whose spectra are produced in Fig. 10, we find

$$2\pi/\bar{\omega}_l = 51 \text{ days.}$$

Dr. Schmitz has provided us with current meter results that are directly comparable; two site mooring records, near (28°N, 69°40′W) and (28°10′N, 68°40′W) respectively were maintained throughout most of the period of the float experiment. From the 578 days of good data at the eastern site, and 596 days at the western site, we find

$$2\pi/\bar{\omega}_e = 54 \text{ days.}$$

Other measures of the time scale of the energy containing eddies (like the first zero-crossing, and the integral scales of the auto-correlation functions) yield the same conclusion: the Lagrangian time-scale is similar to the Eulerian time-scale. This is quite different, from the situation encountered in three dimensional wind tunnel turbulence where fluid particles, in a strong mean flow, retain their velocities longer than does the variety of parcels passing by a fixed anemometer. In this situation the Lagrangian time scale greatly exceeds the Eulerian time-scale (e.g. Monin and Yaglom, 1965). This result is consistent with the level of non-linearity given earlier, in the form of the wave steepness U/C_p, where U is the rms particle speed and C_p the westward pattern speed. However, it should be remembered that C_p is an *upper* bound for the wave phase speed and so the observed value of the ratio $U/C_p = 0.8$ is a lower bound on the wave steepness. Furthermore, the ratio U/C_p, as estimated from Fig. 3a, ranges from about 0.2 to 4, the two measures of non-linearity are therefore in agreement.

The broadening of the Eulerian spectrum relative to the Lagrangian spectrum can more clearly be seen in Fig. 11 with the total Eulerian and Lagrangian spectra plotted so that the area beneath the curves is proportional to kinetic energy. Each of these curves contains about 20 degrees of freedom, and it is evident that the curves are not in fact different at reasonable confidence levels. However, the r.m.s. accelerations are significantly greater in the Eulerian records than in the Lagrangian records. The r.m.s. scalar accelerations are 7.3×10^{-6} and 11.8×10^{-6} cm/sec^2 for the

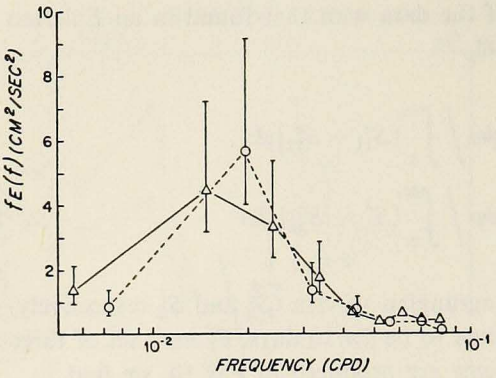

Figure 11. Total Lagrangian and Eulerian power spectra (dashed and solid lines respectively) plotted so that the area beneath the curves is proportional to horizontal kinetic energy.

Lagrangian and Eulerian records respectively. These represent in some sense a quite general statement of the form, 'the Eulerian spectrum has more energy at high frequencies than the Lagrangian spectrum'. If we assume, once again, that 10 days are required for one independent measurement of a statistic, in this case the accelerations, then we can use an F test to reject, at 95% confidence, the hypothesis that the above quoted standard deviations were measured from the same population. In Fig. 7 it can quite clearly be seen that the autocovariance functions are parabolic near the origin, indicating a comparatively large Taylor microscale. The Eulerian autocovariance functions (not shown here) do not show this characteristic curvature, indicating, as above, that significantly larger accelerations are occurring.

The site moorings yield also the Eulerian time-averaged velocities which are (−0.5, −0.3) cm/sec, (western site); (0.1, −0.5) cm/sec, (eastern site). These differ from one another as much as they do from the Lagrangian values, to 1 Jan. 1974, which are (−0.9, −0.3) cm/sec. Clearly the mapping of the mean flows throughout the oceans will be a difficult task. Current meters suffer from mechanical (and fluid mechanical) inaccuracy in measuring residual circulations, while floats, ideally suited in some respects, must still be cautiously interpreted. Their quasi-Lagrangian nature (rather than purely Lagrangian) and the effect of heterogeneous diffusivity require study.

7. Further dynamical statements

We have remarked above that wave-like propagation of patterns can occur in a fluid which is so energetic as to produce cascades of energy between different horizontal and vertical wavenumbers, and that this propagation below the thermocline shows that the Hatteras abyssal plain exists, in a dynamical sense. The two measures of non-linearity already given (wave steepness and the relative difference between Eulerian and Lagrangian time-scales) fall near unity. There is a third, the degree to which the diffusivity of the fluid matches that of a random walk with equivalent time and velocity scales. Due to the shape of the correlation function, Fig. 7, this diffusivity must be classed as efficient (with a band-limited wave field the integral time-scale would vanish) and hence, from this point of view, the flow is rather turbulent.

A north-south particle diffusion has strong dynamical implications on a beta plane.

It tends to be associated with westward turbulent stresses. Various versions of this vorticity mixing process have been discussed by Green (1970), Welander (1973), Rhines (1975 b) and Whitehead (1975). If allowed to operate alone, the planetary vorticity, mixed with the observed diffusivity of 8×10^6 cm^2/sec throughout the water column, implies a westward stress of 0.8 dynes/cm^2. But the primitive models tend to apply far from meridional boundaries; their relevance here has to be demonstrated.

Despite our remarks about nonlinear effects it is worthwhile to speculate how purely linear wave propagation could lead to some of the observed geography of the eddy field. Let us suppose that a wave-like radiation field is produced either by fluctuations in the Gulf Stream shortly after it leaves the Florida Straits, or by reflection of ultra-long planetary waves at the abrupt depth changes west of the MODE area. Furthermore, imagine that this radiation field satisfies the planetary-wave dispersion relation $\omega = -\beta k/(k^2+l^2)$ where the wave function has the form $\exp(i(kx+ly-\omega t))$. If energy is to be propagated away from the source, the group velocity has an eastward component, and

$$\left|\frac{k}{l}\right| = \frac{\text{N/S length scale}}{\text{E/W length scale}} = \left(\frac{\text{N/S velocity variance}}{\text{E/W velocity variance}}\right)^{1/2} > 1.$$

This latter inequality is observed 3.

The suggestion that fluctuations in the Gulf Stream farther north can produce topographic planetary waves, was used by Thompson (1971a, 1971b) to explain the observed, negative u-v correlation at Site D north of the Stream, and to predict that it should be positive south of the Stream. (This prediction was subsequently verified by Schmitz et al., 1975). If this process, or simple reflection, is at work in the MODE area, then the eastward propagating energy will soon encounter the transition from smooth plain to abyssal hills. Back-scattering at the transition seems, on the basis of linear theory, capable of producing the striking drop in intensity seen in Fig. 5. This is particularly true with the shorter waves of small frequency. Some theoretical work tailored to this situation, involving scattering by combinations of bottom slope and rough, three-dimensional topography, is in preparation by Freeland.

A rather different linear theory has been explored by Hall (1974). This involves diffraction of planetary waves from a broken-line model of the western boundary, modelling the shape of the Blake-Bahama outer rise. The ocean floor is otherwise taken to be flat. Hall shows that MODE-1 was really in the near field of this dynamical boundary, that permanent polarization of the particle orbits (tending to line up with the boundary) can occur, and that the shape of the boundary can lead to systematic gradients in kinetic energy of the kinds that we have observed.

We must not, however, overemphasize linear theory and horizontal propagation here, for vertical eddy-eddy interaction is fully capable of creating this kind of deep-ocean flow; in this case the energy source is simply the more vigorous and more ponderous thermocline eddies overhead.

Acknowledgments. The support from the National Science Foundation under grants GX 36342 (P.B.R. and H.F.) and GX 30416 (T.R.) is gratefully acknowledged. We are grateful to the National Center for Atmospheric Research for the use of computing facilities.

REFERENCES

Freeland, H. J. and W. J. Gould. 1976. Objective analysis of meso-scale ocean circulation features. (In preparation).

Green, J. S. A. 1970. Transfer properties of large-scale eddies and the general circulation of the atmosphere. Quarterly Journal R. Met. Soc., *96*: 157–185.

Hall, R. E. 1974. Diffraction of Rossby waves by a wedge-shaped lateral boundary. Notes on the 1974 Summer Study Program in Geophysical Fluid Dynamics at the Woods Hole Oceanographic Institution, WHOI Ref. 74–63, 73–92.

Leaman, K. D. and T. B. Sanford. 1975. Vertical energy propagation of inertial waves: A vector spectral analysis of velocity profiles. J. Geophys. Res. *80*(15): 1975–1978.

Longuet-Higgins, M. S. 1957. The statistical analysis of a random moving surface. Phil. Trans. Roy. Soc. A, *249*: 321–387.

Lumley, J. L. and H. A. Panofsky. 1964. The structure of atmospheric turbulence. Interscience Publishers 239 pp.

Monin, A. S. and A. M. Yaglom. 1966. Statistical Hydromechanics. U.S. Dept. Commerce, Joint Publications Research Service, 605 pp.

Rhines, P. B. 1969. Slow oscillations in an ocean of varying depth. Part I. Abrupt topography. J. Fluid Mech *37*(1): 161–189.

Rhines, P. B. 1975. Waves and turbulence on a β-plane. J. Fluid Mech. *69*(3): 417–443.

Rhines, P. B. 1975 b. Dynamics of unsteady currents. The Sea. Vol. 6. Ed. J. J. O'brien.

Rossby, T., A. D. Voorhis and D. Webb. 1975. A quasi-Lagrangian study of mid-ocean variability using long range SOFAR floats. J. Mar. Res. (This issue).

Schmitz, W. J., J. R. Luyten and W. Sturges. 1975. A note on the spatial variation of the intensity of low frequency fluctuations in the western North Atlantic. (In preparation).

Sverdrup, H. U., M. W. Johnson and R. H. Fleming. 1942. The Oceans: their physics, chemistry and general biology. Prentice-Hall, 1087 pp.

Taylor, G. I. 1921. Diffusion by continuous movements. Proc. Lond. Math. Soc. A, *20*: 196–211.

Thompson, R. 1971a. Topographic Rossby waves at a site north of the Gulf Stream. Deep-Sea Res., *19*(1): 1–19.

Thompson, R. O. R. Y. 1971b. Why there is an intense eastward current in the North Atlantic but not in the South Atlantic. Journ. Phys. Ocean. *2*(3): 235–237.

Welander, P. 1973. Lateral friction in the oceans as an effect of potential vorticity mixing. Geophys. Fl. Dyn. *5*: 173–189.

Whitehead, J. 1975. Mean flows generated by circulation on a beta-plane. Tellus (submitted).

Mode Contribution Number: 40.

Woods Hole Oceanographic Institutions Contribution Number: 3611.

Received: *1 July, 1975.*